Thermochronologic constraints on the origin of the Great Unconformity

Kalin T. McDannell^{a,1}, C. Brenhin Keller^{a,2}, William R. Guenthner^{b,3}, Peter K. Zeitler^{c,4}, and David L. Shuster^{d,e,5}

^a Department of Earth Sciences, Dartmouth College, Hanover, NH 03755; ^bDepartment of Geology, University of Illinois at Urbana-Champaign, Urbana, IL 61801; ^cDepartment of Earth & Environmental Sciences, Lehigh University, Bethlehem, PA 18015; ^dDepartment of Earth & Planetary Science, University of California, Berkeley, CA 94720; ^eBerkeley Geochronology Center, Berkeley, CA 94709

This manuscript was compiled on December 7, 2021

10

11

12

15

20

21

22

23

24

The origin of the phenomenon known as the Great Unconformity has been a fundamental yet unresolved problem in the geosciences for over a century. Recent hypotheses advocate either global continental exhumation averaging 3-5 km during Cryogenian (717-635 Ma) snowball Earth glaciations, or alternatively, diachronous episodic exhumation throughout the Neoproterozoic (1000-540 Ma) due to plate tectonic reorganization from supercontinent assembly and breakup. To test these hypotheses, the temporal pattern of Neoproterozoic thermal histories were evaluated for four North American locations using previously published medium-to-low temperature thermochronology and geologic information. We present inverse time-temperature simulations within a Bayesian modelling framework that record a consistent signal of relatively rapid, high magnitude cooling of ~120-200°C interpreted as erosional exhumation of upper crustal basement during the Cryogenian. These models imply widespread, synchronous cooling consistent with at least \sim 3-5 km of unroofing during snowball Earth glaciations, but also demonstrate that plate tectonic drivers, with the potential to cause both exhumation and burial, may have significantly influenced the thermal history in regions that were undergoing deformation concomitant with glaciation. In the cratonic interior, however, glaciation remains the only plausible mechanism that satisfies the required timing, magnitude, and broad spatial pattern of continental erosion revealed by our thermochronological inversions. To obtain a full picture of the extent and synchroneity of such erosional exhumation, studies on stable cratonic crust below the Great Unconformity must be repeated on all continents.

Great Unconformity | snowball Earth | thermochronology | North America | glacial erosion

ne of the most profound divides in Earth history may be that which separates rocks containing abundant macroscopic fossils from those that do not; a dividing line that is implicit in the name of Earth's current geological Eon—the Eon of visible life, the *Phanerozoic*. For nearly as long as the significance of this dividing line has been appreciated, and before the name Phanerozoic was yet coined (1), it has been associated with another phenomenon—the frequent occurrence of one or more significant unconformities below the oldest rocks containing abundant macroscopic fossils (2). This phenomenon, taking its name from a particularly charismatic occurrence at Grand Canyon (3), has subsequently been referred to by some authors as the *Great Unconformity* (e.g., 4, 5). While lacunae in the geologic record are common (6), those below the oldest rocks of the Phanerozoic are frequently large—in many cases even juxtaposing undeformed sedimentary rocks above, with crystalline igneous or metamorphic basement below (4). The presence of the Great Unconformity in the rock record is significant because the erosion required to create the unconformity and the widespread burial that

preserved it are both equally important. The crucial defining feature of the Great Unconformity is that erosion occurred across a vast area, especially the cratonic interior. The most quantitative reflection of this feature is arguably provided by the coeval step-wise increase in preserved sediment abundance per unit time across the unconformity—a step change first accurately quantified by Ronov and coauthors (7–9), and observed on every continent with the possible exception of Africa. This five-fold discontinuity in global preserved sediment abundance (8) suggests profound changes in both erosional and depositional processes (5), and in any event provides a quantitative metric for the significance of the Great Unconformity as a global feature.

22

23

24

26

27

28

29

30

31

32

33

34

35

36

37

38

39

40

41

42

43

44

45

46

47

The Great Unconformity is, however, far from the only significant phenomenon associated with the emergence of the Phanerozoic world. The transitional Neoproterozoic era saw several significant changes in the Earth system, including the gradual breakup of the supercontinent Rodinia from ~825 Ma to ~570 Ma (10–12), possibly significant fluctuations in atmospheric oxygen (13), and two severe failures of Earth's silicate weathering feedback (14) within the Cryogenian Period (717–635 Ma) that glaciated the continents down to the equator (15, 16). This interval culminated in the Ediacaran Period (635–540 Ma) when the appearance of a more diverse biosphere (e.g., 17), especially macroscopic multicellular organisms, set the stage for the dramatic diversification of visible metazoan life in the earliest Cambrian (18–20). Perhaps the most marked and non-uniformitarian of these events were the

Significance Statement

The Great Unconformity involves a common gap of hundreds of millions to billions of years in the geologic record. The cause of this missing time has long eluded explanation, but recently two opposing hypotheses claim either a glacial or plate tectonic origin in the Neoproterozoic. We provide thermochronologic evidence of rock cooling and multiple kilometers of exhumation in the Cryogenian Period in support of a glacial origin for erosion contributing to the composite basement nonconformity found across the North American interior. The broad synchronicity of this cooling signal at the continental scale can only be readily explained by glacial denudation.

Contributor Roles Taxonomy (CRediT) author statement. KTM: conceptualization, methodology, formal analysis, software, investigation, visualization, interpretation, funding acquisition, project administration, writing-original draft; CBK: conceptualization, methodology, software, writing-original draft, interpretation, funding acquisition, project administration; WRG: validation, funding acquisition, project administration; PKZ: writing-editing, validation, funding acquisition, project administration; DLS: validation, conceptualization.

The authors declare no competing interests.

 $^{^2\}mathrm{To}$ whom correspondence should be addressed. E-mail: kalin.t.mcdannell@dartmouth.edu

hypothesized low-latitude glaciations (15, 16, 21). Maximization of silicate weathering sensitivity due to concentration of Rodinian continents near the equator favored ice-house conditions, and glaciation is thought to have initiated when sea ice advanced within $\sim 40^{\circ}$ of the equator (22). The sea-ice/albedo positive feedback overwhelmed the silicate weathering negative feedback and continental glaciations extended to low latitudes in three episodes, the Sturtian (717–659 Ma), Marinoan (641–635), and Gaskiers (~ 580 Ma)—of which the Sturtian and Marinoan were global 'snowball Earth' events (15, 16, 22–24). The proximal trigger for all three glaciations, however, remains a matter of debate (25–27).

Recently, Keller et al. (5) proposed that widespread erosion by continental ice sheets during these Neoproterozoic glacial intervals may be responsible for the anomalous concentration of unconformities at the end of the Precambrian. If correct, a link between continental glaciation and kilometer-scale cratonic exhumation would have dramatic implications for our understanding of the long-term preservation, composition (via increased sediment subduction and relamination), and freeboard of continental lithosphere, and could help explain a wide set of puzzling observations across several related disciplines (5)—including the much-discussed increase in apparent high-latitude terrigenous sediment flux coincident with Laurentide glaciation (e.g., 28). However, this proposal has not been without controversy (e.g., 29-31). While some of this controversy may be attributable to differences in terminology, significant points of contention remain—primarily, whether Neoproterozoic glaciation did or did not cause significant upper crustal exhumation. Resolving these differences is critical to our understanding of the Neoproterozoic Earth system and the couplings and feedbacks between tectonic, climatic, and biogeochemical processes therein.

Over the past century, the term 'Great Unconformity' has acquired multiple overloaded meanings. Historically, the term was first applied by Clarence Dutton (3) from the rim of the Grand Canyon (USA) to the unconformity at the base of the flat-lying Phanerozoic sedimentary succession within (in some regions a disconformity and in other regions a nonconformity)—though at the time, Dutton did not yet know the true age of the rocks involved. Subsequently, it has been variously used to denote one or more of the following:

- I An unconformity at or near the base of the Phanerozoic, that is separating rocks that contain visible fossils from those that do not (e.g., 2), either in general or at a specific locality.
- II A basement nonconformity, either in general or at a specific locality, often with the (perhaps implicit) additional requirement that the involved basement be Precambrian in age (e.g. 29, 32); or
- III A broader phenomenon evidenced qualitatively by the observation (2, 4) that (I) and (II) frequently coincide (especially relative to what one might expect by chance), suggesting the existence of a globally widespread exposure surface (e.g., 4, 5)—an inference quantitatively confirmed by the global step in preserved sediment abundance first observed by Ronov (8).

This variation in meaning invites confusion and controversy as to the synchroneity or diachroneity of the Great

Unconformity, depending on which (or which combination) of the above meanings is intended. On one hand, individual physical unconformity surfaces are ubiquitously composite in origin, with later episodes of erosion capturing and subsuming previous erosional surfaces. On the other hand, the set of unconformities spanning the base of the Phanerozoic (i.e., I) are in a sense synchronous by definition, as is consequently, to some extent, the broader phenomenon implied in III. Thus, we apply 'Great Unconformity' to the temporal correlation of unconformities in the late Precambrian (III), whereas for example, the usage in Flowers et al. (29) is more aligned with (II)—asserting diachronous worldwide development of many 'Great Unconformities' in the Neoproterozoic.

After accounting for such semantic differences, remaining points of disagreement center on the question of whether or not Neoproterozoic glaciations were significantly erosive. Relatedly, while in no means mutually exclusive with glacial erosion, it also remains entirely worthwhile to quantify the relative contributions to Neoproterozoic crustal exhumation in different regions from such known tectonic events as Rodinia assembly, Rodinia breakup, and Pan-African orogeny. In principle, thermochronology, which allows us to determine time-temperature (and thus exhumation) histories, is well-suited to resolve such questions. However, recent attempts (29–31), taken individually, fall short of truly resolving the critical questions.

Firstly, the uncertainty of time-temperature (t-T) paths derived from a single thermochronometer can be large for older rocks—a problem sometimes exacerbated by the use of suboptimal inversion methodologies—making it difficult to discern between glacial and tectonic drivers by timing alone. Secondly, the magnitude of both glacial and tectonic erosion are expected to be spatially heterogeneous. Fortunately, however, glacial and tectonic processes predict distinct spatial patterns of exhumation—with tectonic erosion focusing in tectonically active regions near cratonic margins, and ice-sheet glacial erosion focusing in regions of wet-based ice—namely, in the models of Donnadieu et al. (33), broad regions of the lowlatitude cratonic interiors away from ice divides, narrowing to a more 'hit-or-miss' pattern at cratonic margins where basal slip is focused into only a few rapid outlet ice streams—as is observed at modern Greenland and Antarctic ice margins. Consequently, in order to resolve the relative contributions of all such climatic and tectonic drivers of erosion in the Neoproterozoic, not to mention their potential interactions, we require higher-resolution t-T paths from localities that can address the spatial pattern of Neoproterozoic exhumation at a global scale. Here we report robust Bayesian thermochronological inversions to test these hypotheses and our results show a widespread pattern of nearly synchronous Cryogenian rock cooling across North America that is interpreted as multiple kilometers of erosional exhumation due to ice-sheet glaciation.

Deep-time thermochronology

Thermochronology allows us to estimate the temperature that a mineral crystal has experienced over time, and its position in the continental crust given a particular thermal structure. It provides a potential test for the contrasting hypotheses regarding the proposed link between widespread glaciation and cratonic exhumation, specifically linking snowball Earth glaciations to the phenomenon of widespread unconformity spanning

the late Neoproterozoic. The use of multiple thermochronometers with varying temperature sensitivities is critical for such deep-time applications, because the parameter space of possible t-T paths only grows with increasing time scale (34). Moreover, although a multichronometer approach can be time-and resource-intensive, the improved resolution critically allows for model results to be independently validated by testing against known geologic constraints, rather than merely forcing the model to fit such constraints a priori.

168

169

170

171 172

173

174

175

176

177

178

181

182

183

184

185

186

187

188

189

190

191

192

193

196

197

198

199

200

201

202

203

205

206

207

208

209

212

213

214

215

216

217

218 219

220

221

222

223

224

227

Recent reports in the thermochronologic literature indicate that nearly continuous thermal histories can be constrained using a multi-method approach (400°C and lower) that involves jointly inverting these data to effectively explore Precambrian histories, supplemented by existing high-temperature metamorphic data and stratigraphic constraints (e.g., 34–37). In this context, the inclusion of medium-temperature (100-300°C) thermochronometers such as K-feldspar ⁴⁰Ar/³⁹Ar and zircon (U-Th)/He are especially important, since lowtemperature systems (< 100°C) tend to record only the most recent Phanerozoic overprints from burial reheating. A robust multichronometer approach featuring a full range of temperature sensitivities, however, should allow us to see past such overprints and accurately constrain the erosion history of ancient crystalline basement over ~Ga timescales. To this end, we consider the following range of thermochronometers:

Potassium feldspar 40 **Ar**/ 39 **Ar dating.** Potassium feldspar is notable for its ubiquity in crustal rocks, for containing appreciable amounts of radiogenic argon, and for containing domains of differing diffusion radius (38). The degassing behavior of domains can be characterized during laboratory 40 Ar/ 39 Ar step-heating experiments and mathematically modeled to determine the number of domains, relative size distribution, and kinetic parameters specific to each sample (39). This information can in turn be inverted to yield a continuous thermal history record between $\sim 350-150^{\circ}$ C (34, 40) and provides a crucial link between high- and low-temperature thermochronometers.

Zircon (ZHe) and apatite (AHe) (U-Th)/He dating. Helium diffusivity in zircon and apatite is modulated by accrued alpharadiation damage from radioactive decay in the crystal lattice (e.g. 41-43). Higher radiation damage in apatite correlates with higher He retentivity (i.e., lower diffusivity; 41). High U zircon grains with greater radiation damage experience faster He diffusion rates over geologic time, whereas the opposite is true for low U grains. Heating of these minerals causes annealing of accumulated radiation damage. Given certain t-Tconditions and mineral chemistries, radiation damage effects manifest as large intra-sample He date variation. Individual grains accumulate a predictable amount of radiation damage as a function of their U and Th concentration and t-T path, and multiple grains from the same sample with different U and Th concentrations will therefore each have a different respective He diffusivity and behave as an independent thermochronometer. The 'effective uranium' of any grain can be represented by the single parameter eU (= $[U]+0.238\times[Th]+0.0012\times[Sm]$; 44), which weights the He contribution from each parent by its alpha-decay productivity. Date-eU trends provide much more powerful and informative thermal history information than any one date (34, 45). The use of many single-crystal dates provides useful information that can be inverted for thermal history, often spanning $\sim 200-40^{\circ}$ C over a range of < 100 ppm to > 2000 ppm eU for zircon, and $\sim 100-50^{\circ}$ C over < 10 ppm to < 200 ppm eU for apatite grains.

228

229

230

231

233

234

235

236

237

238

240

241

242

243

244

245

246

247

248

249

250

251

253

254

255

256

257

258

259

260

261

262

264

265

266

267

268

269

270

272

273

274

275

276

279

280

281

282

283

284

285

Apatite fission-track (AFT) dating. The AFT method is sensitive to temperatures between $\sim 110-60^{\circ}$ C for most rocks that incorporate common apatite, and for this reason is useful for determining upper crustal erosion and burial histories. Fission-track dating is based on quantifying (counting) the damage trails created from the energetic fission of ²³⁸U, which happens continuously at a known rate in the mineral crystal lattice (e.g., 46). These 'fission tracks' are then related to the amount of uranium present in a counted grain area to calculate an apparent 'age' for an apatite grain, or approximate time over which appreciable fission tracks have accumulated in the crystal (47). The production of fission tracks is continuous across a sample's thermal history. Tracks initially have an etched length of $\sim 16-17 \ \mu m$ and shorten with heating, being totally annealed > 120°C (e.g., 48, 49); thus each track has a different age and records a different portion of the thermal history. Annealing resistance is also influenced by apatite chemical composition, notably Cl and other elemental substitutions (50, 51). Track lengths are measured since they can be used to model the style and magnitude of cooling (or partial reheating) experienced during a rock's thermal history (e.g.,

Evaluating published thermochronology data from North America

We examined previously published thermochronology data from the North American interior spread across the continent to adequately test models of the first-order spatial and temporal pattern of Neoproterozoic crustal exhumation (Fig. 1). Data were compiled from the East Lake Athabasca region (Saskatchewan, Canada) (53–55), Archean terranes in the Minnesota River Valley (Minnesota, USA) (43, 56), the Ozark Plateau (Missouri, USA) (36), and the Pikes Peak Batholith (Colorado, USA) (29). The cratonic interior of North America provides an ideal locality for testing the various Great Unconformity formation hypotheses (29) when compared to paleo-margin locations because the craton has remained tectonically stable over the last ~ 1.8 Ga, which alleviates most concerns about more recent, extensive thermal disturbances. In some situations, this allowed us to jointly model samples collected from a broader area of up to 100 km (i.e., Minnesota), under the assumption that over this scale these cratonic rocks have experienced similar thermal histories.

The QTQt software package (63) was used for Bayesian t-T inversion. Thermal-history modelling is often conducted using a simple Monte Carlo approach by searching for and selecting a subset of "acceptable" paths from a finite set of randomly generated t-T paths (e.g., 64). However the large parameter spaces of deep-time thermochronology are arguably better suited to an adaptive inversion methodology such as the reversible-jump Markov chain Monte Carlo (rjMCMC) approach used by QTQt (34). A key aspect of the rjMCMC method as implemented in QTQt is that the complexity of thermal-history solutions is inferred from the data rather than being defined a priori (63, 65). Beyond this, our approach differs from many routine thermochronometric studies by using Bayesian statistical methods for both the search algorithm and data uncertainty treatment, the generation of many more

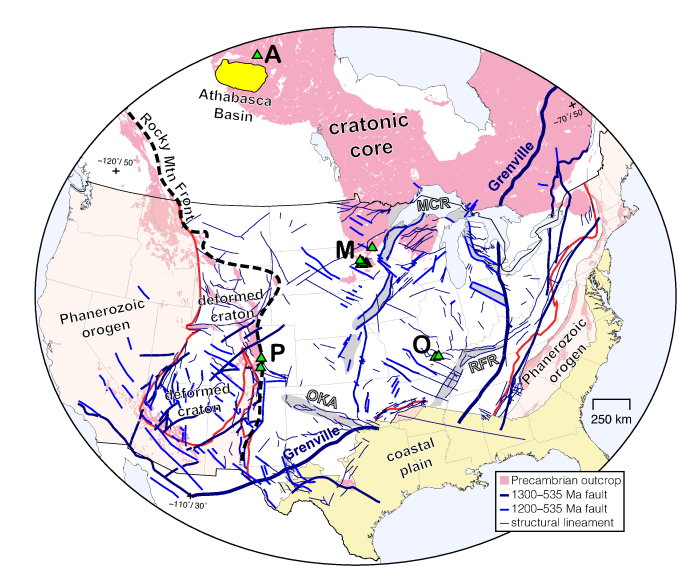


Fig. 1. North American location map for previously published thermochronology datasets discussed in this paper. Sample locations (triangles): A = East Lake Athabasca region; M = Archean Minnesota River Valley terranes; O = Ozark Mountains; P = Pikes Peak batholith. Map shows structural and geologic features of the United States and Canada, adapted from Whitmeyer and Karlstrom (57) and Marshak et al. (58). Precambrian exposed outcrop in pink and Phanerozoic orogens in orange shading. Red lines are the edge of Cenozoic rifting in the west and the Appalachian front in the east from Marshak et al. (58). Major highlighted rifts (gray) that were active in the mid-late Neoproterozoic. MCR = Midcontinent Rift; OKA = Oklahoma aulacogen; RFR = Reelfoot Rift. Note that regional faults were active in the late Neoproterozoic at the Pikes Peak (e.g., 59, 60) and Ozarks locations (e.g., 61), whereas faulting near the Athabasca and Minnesota samples pre-dated Cryogenian time (i.e., ca. 1.9–1.65 Ga (62) and ca. 1.9 Ga Penokean orogeny and/or 1.1 Ga MCR, respectively).

t-T paths (several orders of magnitude) during the course of modelling, and a distinctly empiricist philosophy regarding geologic 'constraint box' implementation (Materials and Methods). That is, we greatly minimize the use of such 'constraint boxes' that force the model to take an expected path, allowing us in such cases to instead observe the ability of the model to independently infer geologically plausible paths from the thermochronologic data alone. We present the resulting t-T histories arranged in order from the cratonic interior outward towards the paleo-Laurentian margins (Fig. 1). The more interior locations generally include more thermochronometric systems, longer modeled time intervals, and are characterized by less interpretive complexity (Fig. 2).

East Lake Athabasca, Canadian Shield, Saskatchewan, Canada. The East Lake Athabasca region lies along the Snowbird Tectonic Zone in the western Canadian Shield at the margin of the remnant ca. 1700–1650 Ma Athabasca Basin (67). High-temperature U–Pb (titanite, apatite, rutile; ~650–400°C) and ⁴⁰Ar/³⁹Ar (hornblende, muscovite, biotite; ~550–300°C) geochronology constrain episodic, post-1900 Ma exhumation of granulites from the deep crust to the surface by 1650 Ma (62). K-feldspar ⁴⁰Ar/³⁹Ar MDD data (~350–150°C) seamlessly link published high- and low-temperature data and establish rapid cooling and exhumation to the near-surface by 1650–1600 Ma (34, 55). Low-temperature thermochronological studies utilizing ZHe, AFT, and AHe data imply thermal resetting and burial heating of the Athabasca region during the late Proterozoic and again during the early Paleozoic (34, 53, 54).

This sample suite was also recently remodeled (without AFT data) in McDannell and Flowers (34) providing similar results using a different t-T search algorithm and different explicit model boundary conditions. This dataset is the most robust out of all the locations studied due to the greater quantity of high-quality thermochronologic data.

Our QTQt thermal history simulations demonstrate rapid cooling to the surface by 1600 Ma, reheating to \sim 120 to <150°C, followed by cooling to surface again from 750–600 Ma (Fig. 2A-B). Minor reheating ensued during Cambro-Ordovician through Devonian time, in agreement with early deposition in the nearby Western Canada Basin. Geologic constraints are enforced in the model at the time of presumed cratonic basement exposure prior to Athabasca Basin formation and at the regional basement nonconformity prior to Paleozoic sedimentation (Fig. 2B). A noteworthy outcome is that the integration of multiple Athabasca thermochronometers containing redundant or complementary kinetic information constrain a broad range of t-T space and yield similar model results for both the 'unconstrained' (Fig. 2A) and 'constrained' (Fig. 2B) models (i.e., no constraint boxes compared to the model with constraint boxes). These t-T models suggest \sim 3–4 km of exhumation during the Sturtian and Marinoan Snowball glaciations in this intracratonic setting (assuming a 25–35°C km⁻¹ paleo-geothermal gradient and 20°C surface temperature; used throughout this paper for any exhumation calculations).

Minnesota River Valley Terranes, Southwestern Minnesota, USA. Minnesota hosts some of the oldest exposed rocks in the United States (Fig. 1), including the 3.5 Ga Morton and Montevideo Gneiss units—both of which are intruded by the 2.6 Ga Sacred Heart Granite (68). Paleoarchean Minnesota River Valley Terranes (MRVT) make up the southernmost extension of the Canadian Superior Province and lie west of the 1100 Ma Midcontinent Rift (MCR) (Fig. 1). The late Proterozoic surface history of the SW Minnesota Archean basement is poorly known, however the preserved Sioux Quartzite to the south of the these samples, is a unit that was deposited at ca. 1760–1630 Ma (69). Regional geologic relationships demonstrate that the Archean crystalline basement was exposed (70) prior to burial during Cambrian through Devonian time, followed by burial again in the Jurassic-Cretaceous (71).

We modelled the ZHe and AHe data reported by Miltich (56) and Guenthner et al. (43). The QTQt model results (Fig. 2C) suggest cooling ensued ca. 750–650 Ma after maximum heating by ca. 800 Ma that obscures the pre-1000 Ma history. It is conceivable that the reheating that concluded by 800 Ma was due to burial by erosional detritus shed from the nearby Grenville orogenic belt (72). The Phanerozoic model history is characterized by Cambrian through Devonian reheating, followed by cooling and a second reheating event that peaks in the Cretaceous, both of which agree with the preserved regional geology (also see SI Appendix; Fig. S1). An amphibolite inclusion from the Sacred Heart Granite dated by C. Naeser in 1974 yielded an AFT age of 460 \pm 45 Ma (1 σ) (73), which is in broad agreement with our Phanerozoic model results showing cooling through the fission-track partial annealing zone (120-60°C) after 500 Ma. These samples are deep in the continental interior and there is no evidence for faulting associated with Rodinia breakup in Minnesota. The effects of 1100 Ma MCR faulting and rifting were localized and would

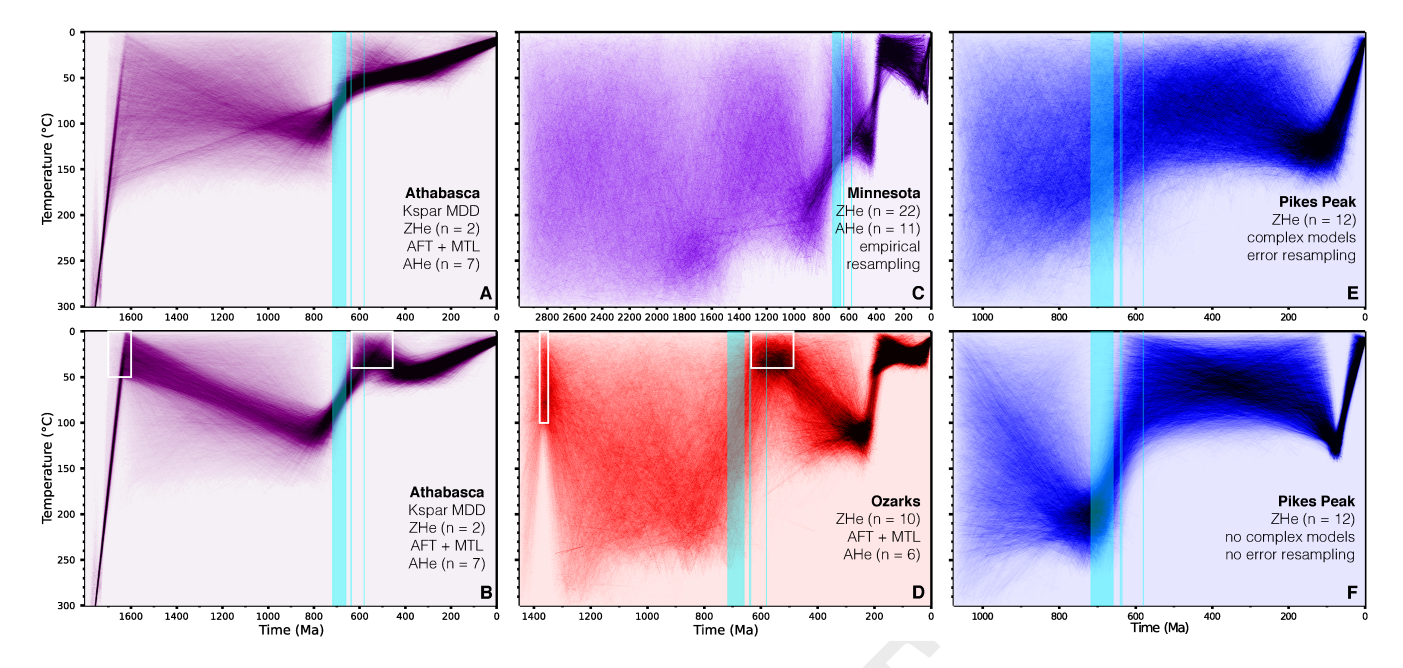


Fig. 2. QTQt time-temperature inversions of thermochronology data from North America. Relative probability is proportional to t-T path density, where darker colors (or higher saturation) denotes higher relative probability. Unless otherwise noted on the panels, Hierarchical Bayes 'error resampling' (63, 66) was implemented within QTQt (scaled from 1-100x; with a value of 1 equal to the input uncertainty) and more complex models were accepted for equivalent likelihood (see Materials and Methods for details). Cvan bars are the time intervals for the respective Sturtian, Marinoan, and Gaskiers glaciations and white t-T boxes are geologic constraints. Plots showing observed and predicted data for each simulation are in the Supplementary Information (SI); Figs. S4-S12. (A-B) Inversion results for East Lake Athabasca (Chipman domain) including the K-feldspar 40 Ar/³⁹ Ar MDD age spectrum reported by McDannell et al. (55) and (U-Th)/He data reported by Flowers et al. (53) and Flowers (54). The modeled ZHe dates are from nearby sample 00-196C a few kilometers away. (A) Model without geologic constraints. (B) Model with a constraint box at 1650 ± 50 Ma between $25 \pm 25^{\circ}$ C, or the time of required basement exposure prior to Athabasca Basin formation (34) and a box at 545 ± 90 Ma and $20 \pm 20^{\circ}$ C to include uncertainty in surface exposure prior to Paleozoic burial onset in the adjoining Western Canada Basin. The Sturtian cooling trend is present in both models, with or without boxes. (C) Inversion results without constraint boxes for the Minnesota River Valley terranes data reported by Miltich (56) and Guenthner et al. (43). A separate model is shown in the SI Appendix; (Fig. S4) implementing geologic constraints of Sioux Quartzite deposition (1695 \pm 65 Ma) and a Precambrian-Cambrian near-surface constraint (600 \pm 100 Ma) prior to Paleozoic burial. The latter box honors the paths at low temperatures in the unconstrained model. The Minnesota ZHe data underwent an empirical form of Hierarchical Bayes resampling (see Materials and Methods and SI Appendix; Fig. S15). (D) Ozarks model result with enforced geologic constraints as described by DeLucia et al. (36), except with an expanded 'Cambrian' box; see text for details. An additional 'no constraint' model is shown in the SI Appendix; Fig. S2. (E-F) Model inversion results for Pikes Peak batholith ZHe data from Flowers et al. (29). (E) More complex models were allowed and data underwent error resampling, whereas in panel (F) dates were randomly sampled within the assigned 10% standard deviation and more complex models were only accepted if they improved model predictions with respect to the input ZHe data. Importantly, the Pikes Peak simulations do not incorporate constraint boxes (refer to Fig. 3 below). An alternate model for Pikes Peak is shown in the SI Appendix; Fig. S3. See SI Appendix for linked QTQt files

have been followed by thermal subsidence. Regardless, all of the MCR events preceded the Cryogenian, thus we anticipate all cooling from $\leq 200^{\circ}\mathrm{C}$ at ca. 720–650 Ma to be associated with > 4 km exhumation resulting from Cryogenian glacial erosion.

Ozark Plateau, St. Francois Mountains, Missouri, USA. The Ozark thermochronology dataset was published by DeLucia et al. (36), who carried out a combination of forward models to test endmember geologic scenarios under different conditions, as well as inverse t-T models to explain their ZHe data. Individual zircon dates were binned by eU and averaged to create 'synthetic' data for use in the HeFTy software (64); also see Pikes Peak section below. They interpreted their HeFTy model results as burial due to Rodinia assembly and Grenville orogenesis from 1200–1000 Ma following by significant Neoproterozoic cooling of $\sim 220-200^{\circ}$ C that they related to the breakup of supercontinent Rodinia. They concluded that exhumation led to increased weathering and CO₂ drawdown, triggering snowball glaciation. Sedimentary burial over the course of the Paleozoic-Mesozoic abruptly ceased with rapid cooling from 225–150 Ma, interpreted as uplift and exhumation from the breakup of supercontinent Pangaea. The Ozark Plateau, like western Colorado (see below), was near the paleo-cratonic margin in the Neoproterozoic-Paleozoic undergoing normal faulting and regional extension (57, 59, 74). This area hosts extensive structural lineament systems and faults, including the Ste. Genevieve, Cottage Grove, and Rough Creek fault zones, the larger Reelfoot Rift (Fig. 1), and the active New Madrid Seismic Zone (58). The \sim 7.5 km of structural relief that exists between the Great Unconformity exposed in the St. Francois Mtns. and the buried Great Unconformity surface in the adjacent Illinois Basin attests to late Precambrian tectonic deformation (58).

399

400

401

402

403

404

405

406

407

408

409

410

411

412

414

415

416

417

418

419

420

Our QTQt inversions are shown with geologic constraints (Fig. 2D) and yield results broadly consistent with those in DeLucia et al. (36), albeit with a greater number of t-T paths generated during the course of modelling and the use of single-grain ZHe data. A model without explicit t-T constraints (SI Appendix; Fig. S2) clearly shows that the thermal event that set the AFT data also obscures the sensitivity of the ZHe data prior to that time. Therefore we used the same modelling constraints as DeLucia et al. (36). Following ca. 1450 Ma granite emplacement from high temperatures, the geologic constraint at 1365 ± 15 Ma and $50 \pm 50^{\circ}$ C represents cooling of surficial rhyolite or hypabyssal granites to near-surface temperatures (Fig. 2D). The late Cambrian Lamotte

376

377

378

379

381

383

384

385

386

387

388

389

390

391

392

393

395

sandstone rests unconformably on the Great Unconformity surface and is represented by the constraint box at 560 ± 75 Ma and $20 \pm 20^{\circ}$ C. Pevehouse et al. (75) suggest weathering and soil formation occurred in the Ozarks after the last major Neoproterozoic glaciation. We have expanded the surface t-T box to include Ediacaran time to account for possible subaerial exposure prior to sandstone deposition (75) and to accommodate elevated Cambrian ocean temperatures (76). The Ozarks ZHe inversion shows reheating between ca. 1300–800 Ma and cooling to surface temperatures by the Cambrian (Fig. 2D). The timing of cooling from peak temperatures of ~ 250 – 200° C is poorly constrained between ca. 800–650 Ma, albeit still consistent with both 'Rodinia breakup' exhumation and snowball Earth glaciations.

422

423

424

425

428

429

430

431

432

434

435

436

437

438

439

440

441

442

443

447

448

449

450

451

452

454

455

456

457

458

459

462

463

464

465

466

467

468

469

470

471

472

473

474

Pikes Peak Batholith, Colorado, USA. Flowers et al. (29) published a ZHe dataset from the Pikes Peak batholith in Colorado (USA). They modelled 'synthetic' ZHe data (see Ozark Plateau section and SI Appendix for further discussion) collected from samples below the Great Unconformity surface and other fault block locations in their study area. Flowers et al. (29) interpreted their t-T results from this single location as unroofing due to global tectonic activity related to supercontinent Rodinia assembly and/or breakup. While such a model would not be incompatible with a glacial model for the origin of the Great Unconformity, given the tectonic activity of the Pikes Peak region in the Neoproterozoic (as shown by fault-bounded nature of many Tavakaiv bodies; see below), several aspects of their interpretation warrant a critical reexamination. Their (29) t-T modelling hinges on assuming shallow emplacement of the enigmatic Tavakaiv quartzite injectites* (60, 78, 79) near the paleosurface at 676 \pm 26 Ma from hematite (U-Th)/He data published by Jensen et al. (80) (Fig. 3A). However, the depth of Tavakaiv emplacement is uncertain due to an unknown emplacement mechanism and the hematite He data can be interpreted as either mineralization or cooling ages (80). The cooling-age interpretation (our preferred model) requires Neoproterozoic burial reheating (80), which is anticipated near Pikes Peak given the striking similarities between detrital zircon U-Pb age distributions for the Tavakaiv dikes and regional Neoproterozoic reference ages (60, 78) (SI Appendix for details). Given the enigmatic nature of Tavakaiv emplacement, their model design could be more accurately described as a compatibility test between the thermochronologic and detrital zircon data; however, the authors presented shallow Tavakaiv emplacement as an a priori constraint and forced their t-Tpaths to conform to this constraint.

Regardless of the interpretive framework to explain the thermochronology data, the t-T models published by Flowers et al. (29) were largely controlled by their use of 'constraint boxes' (81) in the HeFTy software (64) (Fig. 3A). We verified this by generating random Monte Carlo t-T paths using a simple script that only incorporated their constraint boxes without including thermochronologic data (Fig. 3B). In our model (Fig. 3B), random paths were simply forced through

the boxes, yielding the same results as Flowers et al. (29). The box control on modelling is evident from specific placement of their Great Unconformity "exploration field" (Fig. 3A; blue box). This interpretive box (and the other Precambrian boxes) prevent exploration and forced cooling to occur prior to (or by) 720 Ma because paths are required to be between 20–0°C from 1000–720 Ma in the model. There is no physical geologic evidence to support a pre-720 Ma surface condition and it is not demanded by the ZHe data (see SI Appendix for details). We ran additional 'no data' Monte Carlo simulations without Precambrian surface constraints and there are Neoproterozoic cooling paths that satisfy either the glacial or tectonic exhumation hypotheses when not forced to cool to surface temperatures prior to 720 Ma (SI Appendix Fig. S14). The full range of possible t-T paths are also shown after removal of the nested Paleozoic and Mesozoic boxes derived from their assumptions regarding the Pikes Peak history in the Phanerozoic. The example in Figure 2F shows the results of only using the thermochronology data to resolve the thermal history without relying on interpretive t-T boxes.

476

477

478

479

480

481

482

483

484

485

486

487

489

490

491

492

493

494

495

496

497

498

499

500

501

502

503

505

506

507

508

509

510

511

512

514

515

516

517

518

519

520

521

522

523

524

525

526

529

530

531

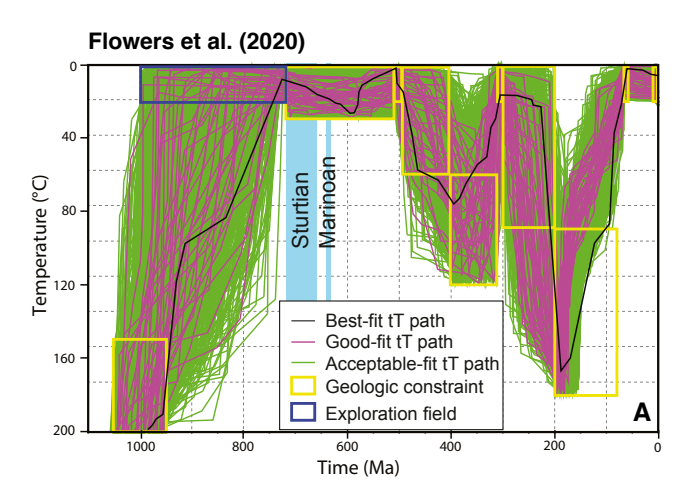
532

533

534

To better understand the thermal history of the Pikes Peak region, we remodelled the Flowers et al. (29) Pikes Peak ZHe dataset using QTQt. Importantly, we applied no constraint boxes; any variations from uniform path density in the results reflects instead the information contained in the 12 measured single-grain ZHe dates from their GU surface samples F1936 and F1937 (29). The resulting t-T history (Fig. 2E-F) exhibits Neoproterozoic cooling from $\sim 220-200^{\circ}\mathrm{C}$ at $\sim 745-700$ Ma to near-surface temperatures by $\sim 660-600$ Ma. The model in Figure 2F is an alternate version where t-T points were only accepted if they resulted in better prediction of the observed dates (i.e., model paths are only as complex as necessary to optimize the data fit between the model and the observations). The latter model is only shown to provide a lower limit on the complexity required to reproduce the ZHe data and reduces noise in Figure 2E. It is obvious that the greatest resolution lies near 200°C at ca. 700–660 Ma (constrained by the oldest ZHe grains), followed by cooling to surface before 600 Ma, and a late reheating event to < 150°C at < 100 Ma, presumably due to burial from the Laramide orogeny. Any heating that may have occurred between 600–100 Ma must be < 150 °C and is not necessarily required or well resolved by the Pikes Peak ZHe data (SI Appendix; Fig. S3). Mid-Paleozoic burial is also not required and basement rocks are not presently mantled by sedimentary cover in the field (29). The Tavakaiv quartzite injectite emplacement age of 676 ± 26 Ma from Jensen et al. (80) and the geologic constraint of basement being exhumed to the surface prior to Sawatch sandstone deposition in the Cambrian are honored in our simulation without imposing t-T constraint boxes (Fig. 2E-F). It is possible that faulting, Tavakaiv emplacement, and basement exhumation were coincident near 700–650 Ma due to Rodinia breakup along the cratonic 'margin' and Snowball ice-sheet dynamics (see the SI Appendix for further discussion). The results of our t-Tinversion for Pikes Peak basement ZHe data offer support for this scenario while still honoring the interpretation of coeval hematite resetting/cooling and injectite emplacement from 200°C to near-surface conditions during the Cryogenian (80). The Neoproterozoic cooling segment in our model is consistent with both the Sturtian and Marinoan glaciations and Rodinia breakup resulting in up to $\sim 5-7$ km of erosional exhumation.

^{*}Flowers et al. (29) maintain that the Tavakaiv injectites contain fragments of Pikes Peak basement that they assert are weathered (i.e., pre-Sturtian) prior to inclusion in the injectite matrix on the basis that the Tavakaiv itself appears "unweathered". However, as a hematitic quartzite, the Tavakaiv is chemically immune to oxidative chemical weathering, so the contrasting weathering extents of the Tavakaiv and the Pikes Peak Granite do not constrain the time of weathering. On the contrary, field relations reveal equivalent degrees of chemical weathering of the susceptible Pikes Peak granite both within and without Tavakaiv dikes (SI Appendix Fig. S13), as part of regional weathering that has long been interpreted as primarily Eocene and later (e.g., 77).



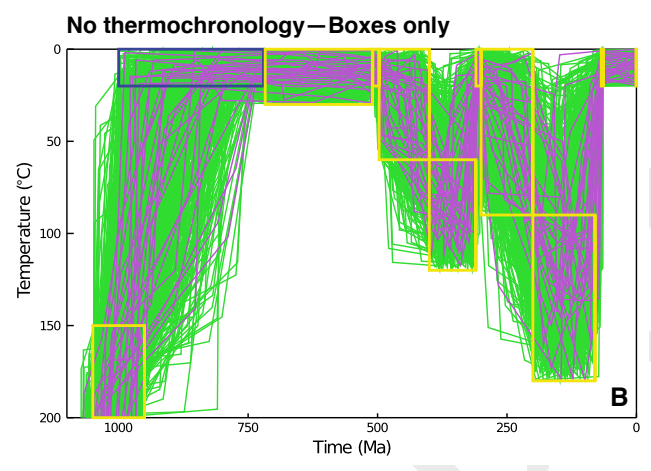


Fig. 3. (A) The Flowers et al. (29) HeFTy (64) time-temperature model for Pikes Peak showing constraints used in their modeling (see text and SI Appendix for discussion of the nature of these constraints). (B) Pure Monte Carlo simulations where a simple script was used to generate random paths to pass through constraint boxes without including thermochronologic data. The simulation in (B) shows 500 randomly drawn paths (green) and a subset of 30 paths (purple) randomly drawn from those 500 to more clearly show overall path behavior. Path colors are only meant to resemble the default HeFTy scheme (64). All boxes are the same as the Flowers et al. (29) model. Our model in (B) only forces paths through boxes and is very similar to the Flowers et al. (29) result (their figure 4 or panel A above). It is important to note that their best-fitting paths (in magenta; panel A) are nearly indistinguishable from a random sampling of 30 of our 500 MC paths. A separate model in the SI Appendix: Fig. S14 shows the result of utilizing only the Phanerozoic geologic constraints and the removal of the Precambrian interpretive boxes, also without thermochronology data. Results show that either early cooling to near surface conditions (i.e., a Rodinia tectonic scenario) or late cooling during a Cryogenian glacial cooling scenario are allowed. Figure 2E-F shows the results of modelling thermochronology data only (without boxes). The model is truncated at 200°C for plotting. The Monte Carlo script is included as a supplemental file.

Reconciling Neoproterozoic exhumation trends

Spatial patterns of tectonic and glacial erosion of continents.

537

539

540

541

542

543

544

547

548

549

550

551

552

554

555

556

557

558

559

560

561

562

565

566

567

568

569

572

573

574

575

576

577

579

580

581

582

583

584

587

590

591

592

593

595

McDannell et al. (55) and DeLucia et al. (36) came to the conclusion that kilometer-scale Neoproterozoic exhumation occurred after 1 Ga within the North American interior and linked this to formation of the Great Unconformity due to Rodinian geodynamics and/or snowball Earth glaciations. These two hypotheses are not mutually exclusive—it is possible that both tectonics and glaciation contributed to global Earth system disruption (82, 83) during formation of the Great Unconformity. Glaciation would be most effective as a driver of erosion in regions with preexisting topography (be it from rifting or orogeny), therefore erosional synergy between tectonics and ice sheets is a possibility (e.g., 84). Ultimately with respect to the Great Unconformity, it may be that the generally accepted reconstruction(s) of more concentrated equatorial packing of the Rodinian continents (11, 85), along with the unique environmental conditions of the Neoproterozoic, proved to be a time of geologic serendipity unlike most any other in Earth history.

Direct and meaningful comparisons between tectonic and glacial unconformity hypotheses are complicated by the fact that there are precise estimates for the timing of Snowball glaciations (23), whereas the timing and duration of Rodinia assembly and breakup remain incompletely understood due to discrepancies between paleomagnetic and geologic data (e.g., 11, 85, 86). Rodinia assembly and breakup occurred episodically and diachronously over at least 250 million years for each phase, with timing dependent upon location (10, 11). Invocation of Rodinian tectonics as a primary, global cause of the Great Unconformity partly requires a consensus or at least reconciliation of the myriad configurations of the supercontinent (e.g., 11, 74, 85, 87–90) to construct valid geodynamic models of uplift during the supercontinent cycle. Otherwise, any thermochronologic cooling signal can simply be attributed to "Rodinian tectonics" in the Neoproterozoic. Notwithstanding Rodinia's exact arrangement, the majority of rift-related deformation and exhumation would have been confined to cratonic margins or to localized horst-graben systems (e.g., 91). A question that arises by appealing to 'tectonics' as a global cause of the Great Unconformity is: why do we not observe an equivalent hiatus as a result of the assembly and breakup of other supercontinents such as Pangaea? If supercontinent cyclicity caused global unconformities akin to the Great Unconformity, we anticipate that the North American Sauk Sequence (as currently defined) would instead occur in the late Mesozoic due to capture by Pangaean erosion. The lull in Pangaean sediment volume (8) during supercontinent breakup is apparently instead due to nondeposition during a sea-level low stand—and is not accompanied by the same stepwise difference in sediment volume that occurs prior to the beginning of the Phanerozoic (5).

The dynamics of supercontinent breakup remain poorly understood (92), but remains a focus of discussion here since the timing of rifting in North America closely overlaps with Snowball glaciations and the timing of cooling in our t-T inversions. Mantle-plume push (i.e., 'bottom-up' processes; 93) and plate boundary dynamics (i.e., subduction retreat or 'top-down' processes; 94) both govern supercontinent breakup (92, 95). Mantle plumes initiate breakup (96), as evidenced by large igneous province eruptions that are either the cause or manifes-

tation of supercontinent demise (92). Successful rifting results in a passive margin and the high number of passive margins during staged Rodinia disassembly (97) implicate Laurentian margin rifting as the dominant mode and locus of tectonic activity during the Neoproterozoic. Longstanding models suggest supercontinents insulate the mantle causing upwelling and breakup (e.g., 98), however recent work suggests that subduction plays a dominant role in subcontinental mantle upwellings (99). Laurentia may not have had well established margin subduction zones until ca. 600–540 Ma (100), which broadly explain the formation (i.e., subduction-related dynamic topography) of North American cratonic unconformities (101) in the Phanerozoic (102)—leaving early Neoproterozoic continental dynamics an open question.

598

599

600

601

603

604

605

606

607

608

611

612

613

614

615

616

619

620

621

622

624

627

628

629

630

631

632

633

634

635

636

637

638

639

644

645

646

647

651

652

653

654

A dynamic topographic response to mantle convection anomalies can produce low amplitude surface uplift (e.g., 103). tilting, and erosion across a continental interior over a few million years (e.g., 104), although this often involves a complex interplay between plate motions and mantle swell position, topography and drainage network organization, and climate change (105)—which are exceedingly difficult to quantify in the Proterozoic. The erosional response to dynamic uplift is proportional to the upwelling wavelength (106); therefore dynamic topography would be required at the scale of the North American continent to induce widespread erosion that agrees with our models. Continental erosion would likely be limited within the interior (< 1–2 km) and occur relatively slowly over many tens of Myr (e.g., 104, 107) in the absence of significant modification of the cratonic lithosphere (e.g., 55). This is considerably less than the amount of unroofing suggested by our t-T models. However speculative, an episode of widespread kilometer-scale epeirogenic uplift associated with a thermally buoyant Rodinia supercontinent (108, 109) may have led to increased continental exposure and the formation of the Great Unconformity on multiple continents. Erosional detritus would have in turn influenced ocean chemistry and atmospheric CO₂ concentrations that contributed to snowball Earth glaciations (22, 110–112).

Conversely, Snowball glaciations could have been the main driver of erosion that created the Great Unconformity. Through a combination of wet-based glacial sliding and lowering of erosional base level, global glaciations in the late Neoproterozoic could have removed several kilometers of rock (including cratonic sedimentary rocks) to produce the Great Unconformity surface. Notably, this would not require incision rates any different than those observed in modern ice-sheet environments. A scenario where modest continental ice sheet incision rates are effectively constant at 0.05 to 0.1 km Myr⁻¹ vields 2.9–5.8 km of exhumation over the Sturtian glacial interval alone. Large amounts of exhumation could be accomplished at either lower rates for prolonged periods of basal ice sliding or more rapidly over short intervals during deglaciation. For example, Cowton et al. (113) indicated that the modern Greenland ice sheet erosion rate is $\sim 2.2-7.4$ km Myr⁻¹ (from the ice margin to > 50 km inland) during the deglacial phase, which is at least an order of magnitude higher than previously established ice sheet erosion rate estimates (114). and places incision rates on par with empirical estimates of ~ 1 to $> 10 \text{ km Myr}^{-1}$ for temperate glaciers (115). The results of Neoproterozoic ice-sheet simulations demonstrate that only high-latitude Rodinian cratons (i.e., not Laurentia) would have

been characterized by cold-based ice; with low-latitude interior basal ice temperatures near 0° C and continental basal sliding displacement rates of ~ 1 to > 10 m yr⁻¹ (33). Furthermore, glacial incision is expected to increase with decreasing latitude (115) and the low-latitude position of Rodinia during the late Neoproterozoic favored increased continental weatherability and precipitation rates (116), thus creating a relationship where erosion would be maximized with lubricated basal ice increasing sliding—leading to more rapid erosion (117).

660

661

662

665

666

667

668

670

673

674

675

676

677

678

680

681

682

683

684

685

688

689

690

691

692

693

696

697

698

699

701

702

703

704

705

706

707

708

709

711

712

713

714

715

716

717

718

719

Cratonic interiors provide the only location to truly test and differentiate the hypotheses of pre-, syn-, or post-Cryogenian formation of the Great Unconformity. Timing is a key component of this signal, but spatial pattern and magnitude of exhumational rock cooling are also critical. Tectonic rifting and glacial erosion will produce opposing spatial patterns of exhumation and different magnitudes of crustal unroofing across a continent. The majority of exhumation associated with supercontinent assembly and breakup would be limited to compressional orogenic belts and extensional (faulted) rift margins, respectively. Rifting will see large exhumation narrowly restricted to continental margins, where tectonic activity is highest, whereas stable continental interiors will experience little to no erosion or even deposition. In addition to orogenic erosion, intraplate stresses manifest as continental extension (e.g., 59), causing subsidence and burial across a craton (118– 120). This is hypothesized for the Rodinian interior during terminal assembly and incipient breakup (e.g., 72) and agrees with the consistent heating signal seen in our thermochronological inversions (Fig. 2). We would expect most tectonic uplift and erosion to occur during early supercontinent assembly and orogenesis, rather than breakup. Thus the rock-cooling signals for Rodinia assembly (ca. 1300–900 Ma; 11), major rift breakup phases (ca. 850–680 Ma; 12, 100), and snowball Earth glaciations (ca. 720–635 Ma) should be rather distinct in terms of timing and location. As an example, recent work by Ricketts et al. (31) apparently shows exhumation that broadly aligns with exhumation during Rodinia assembly in the southwestern USA. While they did not jointly invert $^{40}\mathrm{Ar}/^{39}\mathrm{Ar}$ and zircon (U-Th)/He data, early or episodic Neoproterozoic exhumation may nevertheless be expected locally, since western North America was undergoing active tectonism during that time (e.g., 59).

In contrast, long-term glacial erosion will produce highmagnitude exhumation over areas of 1000s of km², with ice sheet margins either experiencing very little or extremely high incision due to fluctuating ice dynamics and runoff (33, 110). The timing of cooling in our models is coincident with both rifting and glaciation in western North America. We would expect the tectonic versus glacial signals of exhumation on a paleo-cratonic margin (or at least areas experiencing Rodinian syn-rift breakup deformation), to be nearly indistinguishable from one another—as observed in the Pikes Peak region. Locations such as Athabasca are too far from continental margins to have experienced > 3 km of erosion over a short interval solely due to rifting. Moreover, if there is widespread erosion during a 'hard snowball' glaciation, ice would have to be a dominant erosive agent. The only foreseeable way to obtain a consistent, high-magnitude, and synchronous Cryogenian unroofing signal at the continental scale is through ice-sheet glaciation. Our t-T model results demonstrate the viability of such an exhumation pattern across North America.

Deep continental ice-sheet erosion. Widespread, deep Neoproterozoic glacial erosion (121) may appear to contradict the oft-held perception that continental ice sheets cannot deeply erode the upper crust (e.g., 122, 123). Early estimates of physical erosion as a result of the Laurentide glacial episode were that \sim 120 m of rock was removed over the last 3 Myr across upper North America (124), a rate which would equate to some ~ 2.5 km over the duration of the Cryogenian glaciations. However, Laurentide glaciation is perhaps a poor analog to Cryogenian glaciations, since continental freeboard was fundamentally different (i.e., lower) during the Cryogenian, providing a gravitational potential energy gradient essential for deep glacial incision (5). Net base-level fall during snowball Earth termination (and shortly after glaciation) are predicted to be the greatest (up to -600 m) in continental interiors, decreasing towards margins (22), whereas estimates suggest less than -120 m relative sea-level fall during the Laurentide (125). The Laurentide ice divide was positioned over the Hudson Bay Basin where preservation of sedimentary strata was likely due to low rates of basal sliding (126). However, the simple observation that, beyond this ice divide, the thickest parts of the Laurentide ice sheet (e.g., 127) match the currently exposed extent of the Canadian Shield implies that any continental ice sheet is capable of denuding the craton.

720

721

722

723 724

726

727

728

729

730

733

734

735

736

737

738

740

741

742

743

744

747

748

749

750

751

752

753

754

755

756

757

758

759

761

762

763

764

765

766

767

768

769

770

771

772

773

774

775

776

777

An underappreciated aspect of the 'deep erosion' argument is that continental-scale exhumation need not imply that most of the crust removed was crystalline basement; on the contrary, a substantial portion of the eroded crust may well have been intracratonic sedimentary rocks deposited during the Proterozoic across the continental interior (e.g., 72, 128). Geology and our inversions directly indicate burial heating of basement was probably due to thick Proterozoic cover for (at least) the Athabasca region and the Ozark Plateau. In support of this, global average zircon $^{176/177}$ Hf and δ^{18} O isotope anomalies were interpreted as old crustal material from the Earth's surface being subducted and incorporated into new magmas in the Neoproterozoic (5). The Hf and ¹⁸O isotopic signatures only require surface exposure and subduction of crust containing ancient zircons—whether that material was directly sourced from Precambrian basement or recycled from Proterozoic basins makes little difference. Ocean basins serve as the main repository for sediments produced during ice-sheet denudation (121, 124), and due to the shorter oceanic crust lifecycle (compared to continental crust), provide one explanation for the reduced survival rate of Proterozoic detritus that is evident in the Ronov et al. (9) compilations. This conceptually agrees well with the observation that many Archean and Proterozoic terranes have experienced relatively modest amounts of net crustal erosion (129), partially explains the variability and regional lack of evidence for snowball Earth glacial incision (130), and agrees with time-averaged measurements of net continental exhumation rates that approach zero over gigayear timescales (131).

Thermochronologic support for a glacial unconformity

The anomalous abundance of unconformities near the Proterozoic-Phanerozoic boundary—each one different, and frequently composite, but evidently captured by a globally widespread erosive event—are what make the Great Unconformity unique. Neoproterozoic glacial erosion, that we interpret as the primary cause of the Great Unconformity, is detected in

North American thermochronometry without making numerous assumptions about past conditions. We stress that assumptions about past geologic conditions should not be prescribed as evident, or imposed in lieu of quantitative thermochronology in thermal-history models. Our thermochronological inversions honor the measured isotopic data and physical geology, while demonstrating that the late Proterozoic basement nonconformity is a feature that: (i) manifests as large-magnitude erosion between ca. 700–635 Ma, (ii) maintains consistency across North America for multiple locations over a thousand kilometers, and (iii) can be interpreted as widespread (albeit likely spatially heterogeneous) erosional unroofing of at least 3-5 km. Collectively these features can only be readily satisfied by a Cryogenian glacial model for exhumation of rocks sampled from both proximal and distal reaches of exposed Laurentian cratonic basement. It is important to note that this major denudation event does not preclude later, minor sub-kilometer scale erosion (or non-deposition) that undoubtedly occurred across the craton prior to Cambrian flooding of the continent. The removal of $\sim 3-5$ km of thick Mesoproterozoic basin rocks and upper crust from the craton likely caused a disturbance to the stable crustal thermal structure—leaving it warm and isostatically buoyant; thereby inhibiting extensive deposition until Paleozoic transgressions during Pannotia-Gondwana plate reorganization (e.g., 132).

780

781

782

783

784

785

786

787

788

789

790

793

794

795

796

797

798

800

801

802

803

804

806

807

808

809

810

811

813

814

815

816

817

818

819

820

821

822

823

824

825

826

827

828

829

830

831

832

833

834

835

836

837

838

839

840

Development of the Great Unconformity as a physical surface is only constrained in this work between the Cryogenian erosion pulse observed in our t-T models and the age of the overlying sediments—therefore, we do not rule out a multistage or multi-process model for the individual unconformity surfaces associated with the Great Unconformity as a broader phenomenon. However, in order to create and subsequently preserve a widespread unconformity by aggradation, most topographic relief must be removed and the landscape needs to be at (or below) base-level (i.e., 6)—which is difficult to achieve by fluvial or hillslope processes alone. It may be that continental-scale glaciation is the only foreseeable process that can account for both the formation and preservation of the Great Unconformity. Major unconformities, or significant step-changes in North American (or global) sediment abundance are not observed during other times of equatorial continental assembly, potentially invalidating supercontinent tectonic activity as the primary or sole driver of Neoproterozoic exhumation. In our view, it is not a coincidence that the thermochronologic inversions shown here demonstrate nearly synchronous exhumation transpiring across a vast region of North America during a known period of apparent worldwide glaciation. We present a more comprehensive appraisal for the origin of the Great Unconformity within North America that serves as a template for assessing exhumation globally to necessarily test further the hypothesis of a glacial origin due to snowball Earth conditions in the Neoproterozoic.

Materials and Methods

Inverse t-T simulations are presented for samples from the North American interior and were modeled using the QTQt v. 5.8.0 software (63). The QTQt program utilizes Bayesian statistics and a reversible jump Markov chain Monte Carlo (rjMCMC) search method. We modelled K-feldspar 40 Ar/ 39 Ar, zircon (U-Th)/He (ZHe), apatite fission-track (AFT), and apatite (U-Th)/He (AHe) data, implementing the multi-diffusion domain (MDD) model of Lovera et al. (39), zircon radiation damage accumulation and

annealing model (ZRDAAM) of Guenthner et al. (43), the AFT multikinetic annealing model of Ketcham et al. (133), and the AHe radiation damage (RDAAM) kinetic model of Flowers et al. (42) for each respective thermochronometer in our surveyed datasets. To encourage thorough exploration of t-T space, more complex models were accepted for equivalent likelihood and proposal jumps were rejected if they were proposed outside of the general prior (t-T)model space) in QTQt. A total of 1,000,000 models were completed for each example, with 500,000 burn-in iterations that were discarded and an additional 500,000 iterations retained post burn-in for each simulation. The acceptance rates were within the recommended range of \sim 0.2–0.5 and the sampling distribution reached stationarity under these conditions, which collectively signify model convergence

841

842

843

844

846

847

849

851

852

853

854

855

856

857

858

860

862

863

865

867

868

869

870

872

873

874

875

876

877

878

880

881

882

883

885

886

887

888

890

891

892

893

895

897

898

899

901

902

903

905

906

907

908

910

Quantification of data uncertainties. Currently, uncertainties related to eU estimation (e.g., 134), U-Th isotopic zonation (e.g., 135, 136), and imperfect grain geometries are not easily or routinely characterized, therefore it is reasonable to assume that single-grain date uncertainties at the 2σ level are underestimated for both zircon and apatite (U-Th)/He thermochronometry. It is customary for analytical errors to be calculated from the propagated uncertainty from U, Th, and He measurements. Uncertainties are on the order of $\sim 1-5\%$, and typically about 2-3% (137). However, the uncertainties including the Ft correction for alpha ejection are commonly greater, and the reproducibility of laboratory age standards yields total uncertainties nearer to 8-10% for zircon and $\sim 6-7\%$ for apatite (137). These error estimates are more realistic, yet still conservative, and correspond to two standard deviations typically observed on replicate single-grain laboratory age standard Fish Canyon Tuff zircon and Durango apatite analyses (e.g., 134, 137, 138). The age reproducibility estimated for large numbers of replicate analyses of natural AHe samples is much worse, on the order of 15-20% or more (e.g., 139). We usually applied 6% uncertainty for AHe dates (typical Durango apatite reproducibility) and 8-10% for ZHe dates (137) if reported uncertainties were less than these values before modelling. During modelling, dates were randomly sampled from a normal distribution centered on the reported/assigned error (scaled from 1 to 100x the input error), which we refer to as 'error resampling', a form of Hierarchical Bayes resampling utilized in QTQt where the data are used directly for uncertainty inference and the variance of the data errors are estimated from their most probable value, given the data (63, 66). In scenarios where there are abundant, dispersed data of varying quality (i.e., Minnesota dataset), another type of Empirical Bayes resampling was utilized to explore ZHe date uncertainties. The aim was to expand uncertainty accounting where the prior hyperparameters (i.e., observed dates) will have a prior distribution that expresses their initial uncertainty and a posterior distribution that is determined by the data directly (66). The individual date errors were treated as hyperparameters drawn from a probability distribution and the data variance was used to infer date uncertainty. Importantly, observed dates were modeled but the weighted uncertainty was inferred from the scatter of the data as determined by the standard deviation of the data weighted by a Gaussian kernel in eU space ($\sigma eU = 100$ ppm). The empirical Bayes resampling code is available as a Jupyter notebook from https://github.com/kmcdannell/helium-empirical-bayes.git.

Athabasca. We modelled the K-feldspar MDD sample 02-123A from McDannell et al. (55). Refer to McDannell and Flowers (34) for further information on sample data. QTQt modelling information: general prior (t-T model space) 900 \pm 900 Ma and 200 \pm 200°C with an imposed 10°C/Myr maximum heating/cooling rate. Model truncated at $300^{\circ}\mathrm{C}$ for plotting purposes.

Minnesota. We modelled the ZHe and AHe samples contained primarily in the Miltich thesis (56) and Guenthner et al. (43). The Minnesota ZHe samples underwent Empirical Bayes resampling due to the greater number of scattered ZHe (n = 22) dates and the extreme timescale involved in modelling (\sim 2–3x other examples). The majority of reported MRVT (U-Th)/He dates ranged from ca. 925–10 Ma (zircon) and ca. 1725–125 Ma (apatite) (56). Extreme age overdispersion of over 1 Ga affected the apatite grains, which were noted as poor quality by Miltich (56). We refrained from modelling the oldest uncorrected dates because they were typically

characterized by very small grain sizes (~30-40 micron halfwidths) and were much older than the more numerous ca. 300–200 Ma grains. Most raw (no Ft correction) AHe dates ranged from about 270 ± 90 Ma over a range of 37 ± 34 ppm eU. We conservatively applied 10% errors to the MRVT apatites (n = 11 of 16 total analyses) due to the questionable quality of the data—but did not utilize hierarchical error resampling since the dataset likely contains both representative and extreme outlier ages. In this case, error resampling would incorrectly treat all observed dates as reliable, yet more uncertain than initially quantified. The oldest dates were excluded as clear outliers because they were much older than the mean age and during simulation trials they were among the highest misfit grains in the inversions (i.e., grains older than ~ 400 Ma were instead always predicted between ca. 200–350 Ma). The remaining dates form a positive date-eU trend that 'plateaus' at high eU and generally aligns with the RDAAM expectations. QTQt modelling information: general prior (t-T model space) 1500 \pm 1500 Ma and $150\,\pm\,150^{\circ}\mathrm{C}$ with an imposed $5^{\circ}\mathrm{C/Myr}$ maximum heating/cooling rate. Constraint boxes represent Sioux Quartzite deposition at 1695 \pm 65 Ma and 40 \pm 40°C and late Precambrian basement exposure $25 \pm 25^{\circ}\mathrm{C}$ prior to late Cambrian Mt. Simon sandstone deposition $(600 \pm 100 \text{ Ma})$; the unconstrained MRVT model shows solutions at near-surface temperatures during this entire interval; supporting box placement).

913

915

916

918

919

920

921

923

924

925

926

928

929

930

931

933

934

935

936

937

938

939

941

942

943

944

946

947

948

949

950

951

952

953

954

955

957

962

963

964

965

966

968

969

971

972

973

974

975

978

980

981

Ozarks. We remodeled ZHe (samples 14OZ01 and 14OZ11; n = 10), AFT (sample 14OZ07), and AHe data (sample 14OZ11; n = 6) collected from basement below the Great Unconformity surface in the St. Francois Mountains of Missouri from DeLucia et al. (36). The ZHe samples that provided the broadest range in dates and eU were chosen for modelling ($\sim\!1050\text{--}180$ Ma and $\sim\!400\text{--}1800$ ppm eU). The dates from the other samples cluster around $\sim 700-600$ Ma. The AFT sample central age is 185 ± 16 Ma (n = 20) and mean track length is $13.54 \pm 1.23 \ \mu m \ (n=78)$ with a mean Dpar (track etch pit diameter) of 1.75 µm. The AHe sample contains 6 grains (< 15 ppm eU) with dates between $\sim 210-150$ Ma. This information alone signifies heating to temperatures > 100-120°C near 200 Ma to cause thermal resetting of the AFT system followed by relatively rapid cooling through $\sim 110-60^{\circ}\mathrm{C}$. QTQt modelling information: general prior (t-T model space) 725 ± 725 Ma and 150 ± 150 °C with an imposed 5°C/Myr maximum heating/cooling rate. Error resampling (1–100x) for ZHe data and complex models allowed for both scenarios.

Pikes Peak. We remodelled zircon (U-Th)/He data from Pikes Peak samples F1936 and F1937 collected from Great Unconformity surfaces reported by Flowers et al. (29). The 12 single-grain dates span between ${\sim}1000{\text -}45$ Ma and ${\sim}30{\text -}2000$ ppm eU. QTQt modelling information: general prior (t–T model space) 538 \pm 538 Ma and 150 \pm 150°C with an imposed maximum heating/cooling rate of 5°C/Myr. Error resampling (1-100x) for ZHe data and more complex models allowed for Fig. 2E. The Fig. 2F model did not undergo error resampling and more complex models were rejected for equivalent likelihood values. Therefore, proposed t-T paths were only accepted if they provided a better fit to the data.

ACKNOWLEDGMENTS. This work was supported by the NSF Division of Earth Sciences Sedimentary Geo & Paleobiology program awards 2044800 to C.B.K. and K.T.M., 2044603 to P.K.Z., and 2044907 to W.R.G. The Government of Canada Geo-mapping for Energy and Minerals (GEM) Program is recognized by K.T.M. for support during development of these ideas. D.L.S. acknowledges support of the Ann and Gordon Getty Foundation. Thanks to K. Gallagher for QTQt updates and K. Dewing for comments on an earlier version of this manuscript.

- GH Chadwick, Subdivision of geologic time. Bull. Geol. Soc. Am. 41, 47-48 (1930).
- CD Walcott, Cambrian Geology and Paleontology, Smithsonian Miscellaneous Collections. (The Lord Baltimore Press) Vol. 57, (1914).
- CE Dutton, Tertiary History of the Grand Canon District, with Atlas. Monogr. United States
- SE Peters, RR Gaines, Formation of the 'Great Unconformity' as a trigger for the Cambrian explosion. Nature 484, 363-366 (2012).

 CB Keller, et al., Neoproterozoic glacial origin of the Great Unconformity. Proc. Natl. Acad. Sci. 116. 1136–1145 (2019).

982

983

984

985

986

987

988

989

990

991

992

993

994

995

996

997

998

999

1000

1001

1002

1003

1004

1005

1006

1007

1008

1009

1010

1011

1012

1013

1014

1015

1016

1017

1018

1019

1020

1021

1022

1023

1024

1025

1026

1027

1028

1029

1030

1031

1032

1033

1034

1035

1036

1037

1038

1039

1040

1041

1042

1043

1044

1045

1046

1047

1048

1049

1050

1051 1052

1053

1054

1055

1056 1057

1058

1059

1060

1061

1062

1063

1064

1065

- HE Wheeler, Baselevel, lithosphere surface, and time-stratigraphy. Bull. Geol. Soc. Am. 75, 599–610 (1964).
- AB Ronov, VY Khain, AN Balukhovskiy, KB Seslavinskiy, Changes in distribution, volumes, and rates of deposition of sedimentary and volcanogenic deposits during the Phanerozoic (within the present continents). *Int. Geol. Rev.* 19, 1297–1304 (1977).
- AB Ronov, VE Khain, AN Balukhovsky, KB Seslavinsky, Quantitative analysis of Phanerozoic sedimentation. Sedimentary Geol. 25, 311–325 (1980).
- AB Ronov, The Earth's Sedimentary Shell (Quantitative Patterns of its Structure, Compositions, and Evolution): The 20th V.I. Vernadskiy Lecture, March 12,1978. *Int. Geol. Rev.* 24, 1313–1363 (1982).
- JG Meert, TH Torsvik, The making and unmaking of a supercontinent: Rodinia revisited. Tectonophysics 375, 261–288 (2003).
- ZX Li, et al., Assembly, configuration, and break-up history of Rodinia: a synthesis. Precambrian Res. 160, 179–210 (2008).
- ZX Li, DAD Evans, GP Halverson, Neoproterozoic glaciations in a revised global palaeogeography from the breakup of Rodinia to the assembly of Gondwanaland. Sedimentary Geol. 294, 219–232 (2013).
- DB Cole, et al., On the co-evolution of surface oxygen levels and animals. Geobiology 18, 260–281 (2020).
- JCG Walker, PB Hays, JF Kasting, A negative feedback mechanism for the long-term stabilization of Earth's surface temperature. J. Geophys. Res. Ocean. 86, 9776–9782 (1981).
- PF Hoffman, AJ Kaufman, GP Halverson, DP Schrag, A Neoproterozoic Snowball Earth. Science 281, 1342–1346 (1998).
- PF Hoffman, DP Schrag, The snowball Earth hypothesis: testing the limits of global change. Terra Nova 14, 129–155 (2002).
- LM Och, GA Shields-Zhou, The Neoproterozoic oxygenation event: Environmental perturbations and biogeochemical cycling. Earth-Science Rev. 110, 26–57 (2012).
- 18. AH Knoll, The geological consequences of evolution. Geobiology 1, 3-14 (2003).
- AC Maloof, et al., The earliest Cambrian record of animals and ocean geochemical change Geol. Soc. Am. Bull. 122, 1731–1774 (2010).
- EA Sperling, et al., Oxygen, ecology, and the Cambrian radiation of animals. Proc. Natl. Acad. Sci. United States Am. 110, 13446–13451 (2013).
- JL Kirschvink, Late Proterozoic low-latitude global glaciation: the snowball Earth in The Proterozoic Biosphere. (Cambridge University Press), Vol. 52, pp. 51–52 (1992).
- PF Hoffman, et al., Snowball Earth climate dynamics and Cryogenian geology-geobiology. Sci. Adv. 3, e1600983 (2017).
- AD Rooney, JV Strauss, AD Brandon, FA Macdonald, A Cryogenian chronology: Two longlasting synchronous Neoproterozoic glaciations. Geology 43, 459–462 (2015).
- AR Prave, DJ Condon, KH Hoffmann, S Tapster, AE Fallick, Duration and nature of the end-Cryogenian (Marinoan) glaciation. Geology 44, 631–634 (2016).
- 25. E Tziperman, I Halevy, DT Johnston, AH Knoll, DP Schrag, Biologically induced initiation of
- Neoproterozoic snowball-Earth events. *Proc. Natl. Acad. Sci.* **108**, 15091–15096 (2011).

 26. GM Cox, et al., A model for Cryogenian iron formation. *Earth Planet. Sci. Lett.* **433**, 280–292
- (2016).
 FA Macdonald, R Wordsworth, Initiation of Snowball Earth with volcanic sulfur aerosol emissions. *Geophys. Res. Lett.* 44, 1938–1946 (2017).
- P Molnar, Late Cenozoic increase in accumulation rates of terrestrial sediment: How might climate change have affected erosion rates? Annu. Rev. Earth Planet. Sci. 32, 67–89 (2004).
- RM Flowers, FA MacDonald, CS Siddoway, R Havranek, Diachronous development of Great Unconformities before Neoproterozoic Snowball Earth. *Proc. Natl. Acad. Sci. United States* Am. 117, 10172–10180 (2020).
- CP Sturrock, RM Flowers, FA Macdonald, The Late Great Unconformity of the Central Canadian Shield. Geochem. Geophys. Geosystems 22, e2020GC009567 (2021).
- JW Ricketts, et al., Tectonic controls on basement exhumation in the southern Rocky Mountains (United States): The power of combined zircon (U-Th)/He and K-feldspar 40Ar/39Ar thermochronology. Geology 49, 1187–1192 (2021).
- KE Karlstrom, JM Timmons, Many unconformities make one 'Great Unconformity'. Special Pap. Geol. Soc. Am. 489, 73–79 (2012).
- Y Donnadieu, F Fluteau, G Ramstein, C Ritz, J Besse, Is there a conflict between the Neoproterozoic glacial deposits and the snowball Earth interpretation: An improved understanding with numerical modeling. *Earth Planet. Sci. Lett.* 208, 101–112 (2003).
- KT McDannell, RM Flowers, Vestiges of the Ancient: Deep-Time Noble Gas Thermochronology. Elements 16, 325–330 (2020).
- K McDannell, Ph.D. thesis (Theses and Dissertations. 2721, Lehigh University, Bethlehem, Pennsylvania, 261 p.) (2017).
- MS DeLucia, WR Guenthner, S Marshak, SN Thomson, AK Ault, Thermochronology links denudation of the Great Unconformity surface to the supercontinent cycle and snowball Earth. Geology 46, 167–170 (2018).
- KT McDannell, DA Schneider, PK Zeitler, PB O'Sullivan, DR Issler, Reconstructing deep-time histories from integrated thermochronology: An example from southern Baffin Island, Canada. *Terra Nova* 31, 189–204 (2019).
- PK Zeitler, Argon diffusion in partially outgassed alkali feldspars: Insights from 40Ar/39Ar analysis. Chem. Geol. Isot. Geosci. section 65, 167–181 (1987).
- OM Lovera, FM Richter, TM Harrison, The 40Ar/39Ar Thermochronometry for Slowly Cooled Samples Having a Distribution of Diffusion Domain Sizes. J. Geophys. Res. 94, 17917–17935 (1989).
- TM Harrison, M Grove, OM Lovera, PK Zeitler, Continuous Thermal Histories from Inversion of Closure Profiles. Rev. Mineral. Geochem. 58, 389–409 (2005).
- DL Shuster, RM Flowers, KA Farley, The influence of natural radiation damage on helium diffusion kinetics in apatite. Earth Planet. Sci. Lett. 249, 148–161 (2006).
- RM Flowers, RA Ketcham, DL Shuster, KA Farley, Apatite (U-Th)/He thermochronometry using a radiation damage accumulation and annealing model. Geochimica et Cosmochimica

- Acta 73, 2347-2365 (2009).
- WR Guenthner, PW Reiners, RA Ketcham, L Nasdala, G Giester, Helium diffusion in natural zircon: radiation damage, anisotropy, and the interpretation of zircon (U-Th)/He thermochronology. Am. J. Sci. 313, 145–198 (2013).

1066

1067

1068

1069

1070

1071

1072

1073

1074

1075

1076

1077

1078

1079

1080 1081

1082

1083

1084

1085

1086

1087

1088

1089

1091

1092

1093

1095

1096

1097

1098

1099

1100

1101

1102

1103

1104

1105

1106

1107

1108

1109

1110

1111

1112

1113

1114

1115

1116

1117

1118

1119

1120

1121

1122

1123

1124

1125

1126

1127

1128

1129

1130

1131

1132

1133

1134

1135

1136

1137

1138

1139

1140

1141

1142

1143

1144

1145

1146

1147

- EHG Cooperdock, RA Ketcham, DF Stockli, Resolving the effects of 2-D versus 3-D grain measurements on apatite (U-Th)/He age data and reproducibility. *Geochronology* 1, 17–41 (2019).
- AK Ault, WR Guenthner, AC Moser, GH Miller, KA Refsnider, Zircon grain selection reveals (de) coupled metamictization, radiation damage, and He diffusivity. Chem. Geol. 490, 1–12 (2018).
- RL Fleischer, PB Price, RM Walker, Tracks of charged particles in solids. Science 149, 383–393 (1965).
- RA Donelick, PB O'Sullivan, RA Ketcham, Apatite fission-track analysis in Reviews in Mineralogy and Geochemistry. (Mineralogical Society of America) Vol. 58, pp. 49–94 (2005).
- AJ Gleadow, IR Duddy, A natural long-term track annealing experiment for apatite. Nucl. Tracks 5, 169–174 (1981).
- PF Green, IR Duddy, AJW Gleadow, PR Tingate, GM Laslett, Thermal annealing of fission tracks in apatite: 1. A qualitative description. *Chem. Geol. Isot. Geosci. Sect.* 59, 237–253 (1986).
- PF Green, IR Duddy, AJ Gleadow, PR Tingate, GM Laslett, Fission-track annealing in apatite: Track length measurements and the form of the Arrhenius plot. *Nucl. Tracks Radiat. Meas.* (1982) 10, 323–328 (1985).
- WD Carlson, RA Donelick, RA Ketcham, Variability of apatite fission-track annealing kinetics:
 Experimental results. Am. Mineral. 84, 1213–1223 (1999).
- AJ Gleadow, IR Duddy, PF Green, JF Lovering, Confined fission track lengths in apatite: a diagnostic tool for thermal history analysis. *Contributions to Mineral. Petrol.* 94, 405–415 (1986).
- RM Flowers, SA Bowring, PW Reiners, Low long-term erosion rates and extreme continental stability documented by ancient (U-Th)/He dates. Geology 34, 925–928 (2006).
- RM Flowers, Exploiting radiation damage control on apatite (U-Th)/He dates in cratonic regions. Earth Planet. Sci. Lett. 277, 148–155 (2009).
- KT McDannell, PK Zeitler, DA Schneider, Instability of the southern Canadian Shield during the late Proterozoic. Earth Planet. Sci. Lett. 490, 100–109 (2018).
- L Miltich, Low Temperature Cooling History of Archean Gneisses and Paleoproterozic Granites of Southwestern Minnesota. (Carleton College, Northfield, MN. Undergraduate thesis), pp. 1–55 (2005).
- SJ Whitmeyer, KE Karlstrom, Tectonic model for the Proterozoic growth of North America. Geosphere 3, 220–259 (2007).
- S Marshak, et al., The basement revealed: Tectonic insight from a digital elevation model of the Great Unconformity, USA cratonic platform. Geology 45, 391–394 (2017).
- JM Timmons, KE Karlstrom, CM Dehler, JW Geissman, MT Heizler, Proterozoic multistage (ca. 1.1 and 0.8 Ga) extension recorded in the Grand Canyon Supergroup and establishment of northwest- and north-trending tectonic grains in the southwestern United States. Geol. Soc. Am. Bull. 113, 163–181 (2001).
- CS Siddoway, GE Gehrels, Basement-hosted sandstone injectites of Colorado: A vestige
 of the Neoproterozoic revealed through detrital zircon provenance analysis. *Lithosphere* 6,
 403–408 (2014).
- CJ Potter, JA Drahovzal, ML Sargent, JH McBride, Proterozoic structure, cambrian rifting, and younger faulting as revealed by a regional seismic reflection network in the Southern Illinois Basin. Seismol. Res. Lett. 68, 537–552 (1997).
- RM Flowers, et al., Multistage exhumation and juxtaposition of lower continental crust in the western Canadian Shield: Linking high-resolution U-Pb and40Ar/39Ar thermochronometry with pressure-temperature-deformation paths. *Tectonics* 25, 1–20 (2006).
- K Gallagher, Transdimensional inverse thermal history modeling for quantitative thermochronology. J. Geophys. Res. Solid Earth 117 (2012).
- RA Ketcham, Forward and inverse modeling of low-temperature thermochronometry data in Reviews in Mineralogy and Geochemistry. (Mineralogical Society of America) Vol. 58, pp. 275–314 (2005).
- KT McDannell, DR Issler, Simulating sedimentary burial cycles Part 1: Investigating the role
 of apatite fission track annealing kinetics using synthetic data. Geochronology 3, 321–335
 (2021).
- A Malinverno, VA Briggs, Expanded uncertainty quantification in inverse problems: Hierarchical Bayes and empirical Bayes. Geophysics 69, 1005–1016 (2004).
- 67. RH Rainbird, RA Stern, N Rayner, CW Jefferson, Age, provenance, and regional correlation of the Athabasca Group, Saskatchewan and Alberta, constrained by igneous and detrital zircon geochronology. *Bull. - Geol. Surv. Can.* 588, 193 (2007).
- ME Bickford, JL Wooden, RL Bauer, SHRIMP study of zircons from Early Archean rocks in the Minnesota River Valley: Implications for the tectonic history of the Superior Province. *Bull. Geol. Soc. Am.* 118, 94–108 (2006).
- DL Southwick, GB Morey, JH Mossler, Fluvial origin of the lower Proterozoic Sioux quartzite, southwestern Minnesota. Geol. Soc. Am. Bull. 97, 1432–1441 (1986).
- LG Medaris, et al., Anatomy of a sub-cambrian paleosol in Wisconsin: Mass fluxes of chemical weathering and climatic conditions in North America during formation of the Cambrian great unconformity. J. Geol. 126, 261–283 (2018).
- 71. MA Jirsa, et al., S-21 Geologic Map of Minnesota-Bedrock Geology (2011).
- RH Rainbird, LM Heaman, G Young, Sampling Laurentia: Detrital zircon geochronology offers evidence for an extensive Neoproterozoic river system originating from the Grenville orogen. *Geology* 20, 351–354 (1992).
- BR Doe, MH Delevaux, Lead-isotope investigations in the minnesota river valley- Late-tectonic and posttectonic granites. Special Pap. Geol. Soc. Am. 182, 105–112 (1980).
- KE Karlstrom, et al., Refining Rodinia: Geologic evidence for the Australia-Western U.S. Connection in the Proterozoic. GSA Today 9, 2–7 (1999).
- KJ Pevehouse, et al., Paleotopography controls weathering of Cambrian-age profiles beneath the great unconformity, St. Francois Mountains, SE Missouri, U.S.A. J. Sedimentary Res. 90,

1150 629-650 (2020).

1151

1152

1153

1154

1155

1156

1157

1158

1159

1160

1161

1162

1163

1164

1165

1166

1167

1168

1169

1170

1175

1176

1177

1178

1179

1180

1181

1182

1183

1184

1188

1189

1190

1191

1192

1193

1194

1195

1196

1197

1198

1199

1200

1201

1202

1203

1204

1206

1207

1208

1209

1224

1225

1226

1227

1228 1229

1230

- KD Bergmann, et al., A paired apatite and calcite clumped isotope thermometry approach to estimating Cambro-Ordovician seawater temperatures and isotopic composition. Geochimica et Cosmochimica Acta 224, 18–41 (2018).
- 77. T Steven, E Evanoff, R Yuhas, D Bolyard, S Sonnenberg, Middle and late Cenozoic geomorphic development of the Front Range of Colorado in Geologic History of the Colorado Front Range: Rocky Mountain Section, American Association of Petroleum Geologists, Field Trip Guidebook. (Rocky Mountain Association of Geologists), pp. 28–30 (1997).
- C Siddoway, P Myrow, E Fitz-Diaz, Strata, structures, and enduring enigmas: A 125th Anniversary appraisal of Colorado Springs geology in Classic Concepts and New Directions: Exploring 125 Years of GSA Discoveries in the Rocky Mountain Region, eds. L Abbott, G Hancock. (Geological Society of America), pp. 331–356 (2013).
- CS Siddoway, G Palladino, G Prosser, D Freedman, WC Duckworth, Basement-hosted sand injectities: use of field examples to advance understanding of hydrocarbon reservoirs in fractured crystalline basement rocks. *Geol. Soc. London, Special Publ.* 493, 493–2018 (2019).
- JL Jensen, et al., Single-crystal hematite (U–Th)/He dates and fluid inclusions document widespread Cryogenian sand injection in crystalline basement. Earth Planet. Sci. Lett. 500, 145–155 (2018).
- P Vermeesch, Y Tian, Thermal history modelling: HeFTy vs. QTQt. Earth-Science Rev. 139, 279–290 (2014).
- 1171 82. Y Goddéris, et al., The Sturtian 'snowball'glaciation: fire and ice. Earth Planet. Sci. Lett. 211, 1172 1–12 (2003).
- 83. TM Gernon, TK Hincks, T Tyrrell, EJ Rohling, MR Palmer, Snowball Earth ocean chemistry
 driven by extensive ridge volcanism during Rodinia breakup. Nat. Geosci. 9, 242–248 (2016).
 - A Walsh, T Ball, DM Schultz, Extreme sensitivity in Snowball Earth formation to mountains on PaleoProterozoic supercontinents. Sci. Reports 9 (2019).
 - AS Merdith, et al., A full-plate global reconstruction of the Neoproterozoic. Gondwana Res. 50, 84–134 (2017).
 - KE Karlstrom, et al., Chuar Group of the Grand Canyon: Record of breakup of Rodinia, associated change in the global carbon cycle, and ecosystem expansion by 740 Ma. *Geology* 28, 619–622 (2000).
 - EM Moores, Southwest US-East Antarctic (SWEAT) connection: a hypothesis. Geology 19, 425–428 (1991)
 - SA Pisarevsky, MT Wingate, CM Powell, S Johnson, DA Evans, Models of Rodinia assembly and fragmentation. Geol. Soc. Special Publ. 206, 35–55 (2003).
- and fragmentation. Geol. Soc. Special Publ. 206, 35–55 (2003).
 By DA Evans, The palaeomagnetically viable, long-lived and all-inclusive Rodinia supercontinent reconstruction. Geol. Soc. Special Publ. 327, 371–404 (2009).
 - X Jing, et al., Inverted South China: A novel configuration for Rodinia and its breakup. Geology 49, 463–467 (2021).
 - KE Karlstrom, M Heizler, MC Quigley, Structure and 40Ar/39Ar K-feldspar thermal history of the Gold Butte block: Reevaluation of the tilted crustal section model in *Miocene Tectonics of* the Lake Mead Region, Central Basin and Range, eds. PJ Umhoefer, LS Beard, MA Lamb. (Geological Society of America Special Paper 463, Boulder, CO, United States), pp. 331–352
 - 92. RN Mitchell, et al., The supercontinent cycle. Nat. Rev. Earth Environ. 2, 358–374 (2021).
 - JB Murphy, RD Nance, Speculations on the mechanisms for the formation and breakup of supercontinents. Geosci. Front. 4, 185–194 (2013).
 - PA Cawood, RA Strachan, SA Pisarevsky, DP Gladkochub, JB Murphy, Linking collisional and accretionary orogens during Rodinia assembly and breakup: Implications for models of supercontinent cycles. Earth Planet. Sci. Lett. 449, 118–126 (2016).
 - M Gurnis, Large-scale mantle convection and the aggregation and dispersal of supercontinents. Nature 332, 695

 –699 (1988).
 - N Zhang, Z Dang, C Huang, ZX Li, The dominant driving force for supercontinent breakup: Plume push or subduction retreat? *Geosci. Front.* 9, 997–1007 (2018).
- 97. DC Bradley, Passive margins through earth history. *Earth-Science Rev.* **91**, 1–26 (2008).
 - DL Anderson, Hotspots, polar wander, Mesozoic convection and the geoid. Nature 297, 391 (1982).
 - PJ Heron, JP Lowman, The impact of Rayleigh number on assessing the significance of supercontinent insulation. J. Geophys. Res. Solid Earth 119, 711–733 (2014).
- 1210 100. AS Merdith, SE Williams, S Brune, AS Collins, RD Müller, Rift and plate boundary evolution
 1211 across two supercontinent cycles. Glob. Planet. Chang. 173, 1–14 (2019).
- 1211 across two supercontinent cycles. Glob. Planet. Chang. 173, 1–14 (2019).
 1212 101. LL Sloss, Sequences in the Cratonic Interior of North America. Geol. Soc. Am. Bull. 74, 93
 (1963)
- 102. PM Burgess, M Gurnis, L Moresi, Formation of sequences in the cratonic interior of North
 America by interaction between mantle, eustatic, and stratigraphic processes. *Bull. Geol.* Soc. Am. 109, 1515–1535 (1997).
- 103. N Flament, M Gurnis, RD Muller, A review of observations and models of dynamic topography
 Lithosphere 5. 189–210 (2013).
- 1219 104. J Braun, F Guillocheau, C Robin, G Baby, H Jelsma, Rapid erosion of the Southern African
 Plateau as it climbs over a mantle superswell. J. Geophys. Res. Solid Earth 119, 6093–6112
 (2014).
- 105. GA Ruetenik, R Moucha, GD Hoke, Landscape response to changes in dynamic topography.
 Terra Nova 28, 289–296 (2016).
 - J Braun, X Robert, T Simon-Labric, Eroding dynamic topography. Geophys. Res. Lett. 40, 1494–1499 (2013).
 - 107. JR Stanley, RM Flowers, DR Bell, Erosion patterns and mantle sources of topographic change across the southern African Plateau derived from the shallow and deep records of kimberlites. Geochem. Geophys. Geosystems 16, 3235–3256 (2015).
 - ZX Li, XH Li, PD Kinny, J Wang, The breakup of Rodinia: did it start with a mantle plume beneath South China? Earth Planet. Sci. Lett. 173, 171–181 (1999).
- 109. ZX Li, et al., Geochronology of Neoproterozoic syn-rift magmatism in the Yangtze Craton,
 South China and correlations with other continents: evidence for a mantle superplume that
 broke up Rodinia. Precambrian Res. 122, 85–109 (2003).

 Y Donnadieu, Y Goddéris, G Ramstein, A Nédélec, J Meert, A 'snowball Earth' climate triggered by continental break-up through changes in runoff. Nature 428, 303–306 (2004). 1234

1235

1236

1237

1238

1239

1240

1241

1242

1243

1244

1245

1246

1247

1248

1249

1250

1251

1252

1253

1254

1255

1256

1257

1258

1259

1260

1261

1265

1266

1268

1269

1270

1271

1272

1273

1274

1275

1276

1277

1278

1279

1280

1281

1282

1283

1284

1285

1286

1287

1288

1289

1290

1291

1292

1293

1294

1295

1296

- Y Goddéris, et al., Coupled modeling of global carbon cycle and climate in the Neoproterozoic: links between Rodinia breakup and major glaciations. *Comptes Rendus Geosci.* 339, 212–222 (2007).
- GM Cox, et al., Continental flood basalt weathering as a trigger for Neoproterozoic Snowball Earth. Earth Planet. Sci. Lett. 446. 89–99 (2016).
- T Cowton, P Nienow, I Bartholomew, A Sole, D Mair, Rapid erosion beneath the Greenland ice sheet. Geology 40, 343–346 (2012).
- B Hallet, L Hunter, J Bogen, Rates of erosion and sediment evacuation by glaciers: A review of field data and their implications. Glob. Planet. Chang. 12, 213–235 (1996).
- M Koppes, et al., Observed latitudinal variations in erosion as a function of glacier dynamics. Nature 526, 100–103 (2015).
- FA Macdonald, NL Swanson-Hysell, Y Park, L Lisiecki, O Jagoutz, Arc-continent collisions in the tropics set Earth's climate state. Science 364, 181–184 (2019).
- 117. SJ Cook, DA Swift, MP Kirkbride, PG Knight, RI Waller, The empirical basis for modelling glacial erosion rates. *Nat. Commun.* 11, 1–7 (2020).
- MHP Bott, Origin of lithospheric tension causing basin formation. *Philos. Trans. R. Soc. Lond.* 305, 319–324 (1982).
- PA Allen, JJ Armitage, Cratonic basins in Tectonics of sedimentary basins: Recent advances, eds. C Busby, A Azor. (Wiley), First edition, pp. 602–620 (2012).
- PM Burgess, Phanerozoic Evolution of the Sedimentary Cover of the North American Craton in The Sedimentary Basins of the United States and Canada. (Elsevier) Vol. 5, pp. 39–75 (2019).
- WA White, Deep erosion by continental ice sheets. Bull. Geol. Soc. Am. 83, 1037–1056 (1972).
- 122. CP Gravenor, Erosion by continental ice sheets. Am. J. Sci. 275, 594-604 (1975).
- 123. DE Sugden, Glacial Erosion by the Laurentide Ice Sheet. J. Glaciol. 20, 367-391 (1978).
- M Bell, EP Laine, Erosion of the Laurentide region of North America by glacial and glaciofluvial processes. Quat. Res. 23, 154–174 (1985).
- EJ Gowan, et al., A new global ice sheet reconstruction for the past 80 000 years. Nat. Commun. 12, 1–9 (2021).
- JM Licciardi, PU Clark, JW Jenson, DR Macayeal, Deglaciation of a soft-bedded Laurentide loe Sheet. Quat. Sci. Rev. 17, 427–448 (1998).
- D Lacelle, DA Fisher, S Coulombe, D Fortier, R Frappier, Buried remnants of the Laurentide Ice Sheet and connections to its surface elevation. Sci. Reports 8, 1–10 (2018).
- JA Fraser, LP Tremblay, Correlation of Proterozoic strata in the northwestern Canadian Shield. Can. J. Earth Sci. 6, 1–9 (1969).
- D Abbott, et al., Quantifying Precambrian crustal extraction: the root is the answer. Tectonophysics 322, 163–190 (2000).
- RN Mitchell, et al., Hit or miss: Glacial incisions of snowball Earth. Terra Nova 31, 381–389 (2019).
- TJ Blackburn, et al., An Exhumation History of Continents over Billion-Year Time Scales. Science 335, 73–76 (2012).
- IW Dalziel, Cambrian transgression and radiation linked to an lapetus-Pacific oceanic connection? Geology 42, 979–982 (2014).
- RA Ketcham, A Carter, RA Donelick, J Barbarand, AJ Hurford, Improved modeling of fissiontrack annealing in apatite. Am. Mineral. 92, 799

 –810 (2007).
- WR Guenthner, PW Reiners, U Chowdhury, Isotope dilution analysis of Ca and Zr in apatite and zircon (U-Th)/He chronometry. Geochem. Geophys. Geosystems 17, 1623–1640 (2016).
- KA Farley, DL Shuster, RA Ketcham, U and Th zonation in apatite observed by laser ablation ICPMS, and implications for the (U-Th)/He system. Geochimica et Cosmochimica Acta 75, 4515–4530 (2011).
- AK Ault, RM Flowers, Is apatite U–Th zonation information necessary for accurate interpretation of apatite (U–Th)/He thermochronometry data? Geochimica et Cosmochimica Acta 79, 60–78 (2012).
- PW Reiners, S Nicolescu, Measurement of parent nuclides for (U-Th)/He chronometry by solution sector ICP-MS, (University of Arizona), Technical report (2006).
- PW Reiners, TL Spell, S Nicolescu, KA Zanetti, Zircon (U-Th)/He thermochronometry: He diffusion and comparisons with 40 Ar/39 Ar dating. Geochimica et Cosmochimica Acta 68, 1857–1887 (2004).
- 139. KT McDannell, PK Zeitler, DG Janes, BD Idleman, AK Fayon, Screening apatites for (U-Th)/He thermochronometry via continuous ramped heating: He age components and implications for age dispersion. Geochimica et Cosmochimica Acta 223, 90–106 (2018).